symmetry

MDPI

Article

Effect of Aspect Ratio on Optimal Disturbances of Duct Flows

Andrey Boiko [1,2,*], Kirill Demyanko [2,3] and Nikita Klyushnev [3]

1 Khristianovich Institute of Theoretical and Applied Mechanics, Russian Academy of Sciences, 4/1 Institutskaya Str., Novosibirsk 630090, Russia
2 Marchuk Institute of Numerical Mathematics, Russian Academy of Sciences, Gubkin Str., 8, Moscow 119333, Russia; k.demyanko@inm.ras.ru
3 Keldysh Institute of Applied Mathematics, Russian Academy of Sciences, Miusskaya Sq., 4, Moscow 125047, Russia; n_klyushnev@mail.ru
* Correspondence: boiko@itam.nsc.ru

Abstract: The linear temporal stability of the Poiseuille flow through a rectangular duct is considered. The effect of the duct aspect ratio on the transient growth of disturbances, which causes the so-called subcritical laminar–turbulent transition, is studied numerically. In particular, it is shown that an increase in the aspect ratio promotes the subcritical transition in almost the entire considered range of the duct aspect ratios except a relatively narrow range, where the increase suppresses the transient growth of disturbances. Such peculiarity is qualitatively explained by considering the nonmodal stability of more simplified plane channel flow.

Keywords: linear hydrodynamic stability; nonmodal instability; optimal disturbances; symmetries of disturbances; viscous duct flows

check for updates

Citation: Boiko, A.; Demyanko, K.; Klyushnev, N. Effect of Aspect Ratio on Optimal Disturbances of Duct Flows. *Symmetry* **2023**, *15*, 2121. https://doi.org/10.3390/sym15122121

Academic Editor: Artur V. Dmitrenko

Received: 29 October 2023
Revised: 25 November 2023
Accepted: 26 November 2023
Published: 28 November 2023

1. Introduction

Viscous incompressible fluid flows in ducts and pipes are encountered in many engineering and biotechnology applications. Therefore, it is of great interest to study the influence of various factors on the stability of such flows in order to develop methods for passive control of their stability characteristics. One of such factors is the ratio the flow geometric scales in the cross–flow plane. For example, for the Poiseuille flow in a rectangular duct, the dependence of the linear critical Reynolds number, $\mathrm{Re_L}$, which determines the boundary of the asymptotic Lyapunov stability [1] of a given basic flow, on the duct aspect ratio A is computed [2] and qualitatively explained [3]. In particular, it is shown that this flow is linearly stable at $A < A_c \approx 3.2$, that is $\mathrm{Re_L} = \infty$. With further increase in A, the flow became linearly unstable with $\mathrm{Re_L}$ tending to $\mathrm{Re_L} \approx 5772$ [4] for the plane Poiseuille flow. For the Poiseuille flow in a pipe of axially uniform elliptic cross-section the dependence $\mathrm{Re_L}(A)$ is qualitatively similar to that in the rectangular duct, though with $A_c \approx 10.4$ [5]. In addition, later it has been shown for this flow that the energy-critical Reynolds number, $\mathrm{Re_E}$, which is the lower limit of the Reynolds numbers enabling the growth of disturbance kinetic energy, noticeably depends on A [6] as well.

At the Reynolds numbers, Re, larger than $\mathrm{Re_L}$, flows are usually turbulized due to the growth in time (temporal instability) or in space (spatial instability) of individual unstable modes (modal instability). Nevertheless, flows may also lose their stability at $\mathrm{Re_E} < \mathrm{Re} < \mathrm{Re_L}$ due to the significant transient growth of the kinetic energy of disturbances (nonmodal instability) [7,8]. From the mathematical point of view, such growth of disturbance kinetic energy is possible if the amplitudes of the modes comprising the disturbance are non-orthogonal, i.e., the operator of the linearized equations for disturbance amplitudes is non-normal [9–13]. The maximum amplification of the kinetic energy of disturbances is achieved by the so-called optimal disturbances, which are a superposition of a large number of essentially non-orthogonal modes. A comprehensive description of the theory of nonmodal instability, as well as a review of known results, can be found in [7,8,14,15].

In this paper, the Poiseuille flow in an infinite duct of streamwise-uniform rectangular cross-section is considered. The linear nonmodal instability of this flow is numerically investigated in the temporal framework (in contrast to works [2,3] studying the modal temporal instability of this flow). In particular, the influence of the duct aspect ratio on the maximum amplification of the kinetic energy of disturbances as well as on the form of the optimal disturbances is examined. This study is carried out taking into account possible symmetries with respect to the cross-section axes, which are possessed by solutions of the linearized equations for disturbance amplitudes. Accounting for the symmetries significantly reduces computational costs and memory requirements for the computation of stability characteristics as well as facilitates the analysis and interpretation of the obtained results.

The present study provides a better understanding of the effect of ratio of flow geometric scales in the cross-flow direction on the nonmodal instability of shear flows in ducts and pipes, which usually manifests itself as the subcritical laminar–turbulent transition. In addition, the problem under consideration deserves attention as the rectangular ducts are typical requisites for heat exchangers and heating, ventilation and air-conditioning systems [16–18]. The heat and mass transfer of such flows depends significantly on whether the flow is laminar or turbulent. According to the specific application, it may be preferred either to suppress the flow instabilities to reduce vorticity (thereby reducing hydraulic drag [19,20] and enhancing mass transfer) or to advance the transition to turbulence to enhance mixing and heat transfer. Thus, the results of present study may be useful in the design of these engineering devices.

Note that a limitation of the this study is the adoption of the temporal framework (when a disturbance is given at an initial moment in the entire duct and the temporal evolution of this disturbance is investigated) instead of the spatial one (when the disturbance is given in some cross-section of the duct and the downstream propagation of this disturbance is investigated). The latter is more realistic, but the results of Criminale et al. [21] and Lasseigne et al. [22] suggest the existence of a transform relating temporal transient with the spatial one (see, e.g., discussion of the Formulas (26)–(28) in [21]). Therefore it is expected that the spatial stability analysis provides qualitatively the same results.

This paper has the following structure. Section 2.1 formulates the problem of the nonmodal stability, including the linearized equations for disturbance amplitudes. Section 2.2 describes the differential-algebraic system arising after the spatial approximation of these equations by a spectral collocation method. Then, the algebraic reduction of this system, proposed and justified in [23,24], is discussed. It allows one to reduce the system to an equivalent system of ordinary differential equations of approximately half the algebraic dimension. In addition, this section describes accounting for the symmetries of disturbances at the matrix level. Section 3 presents the results of the study. Section 4 summarizes the paper.

2. Materials and Methods

2.1. Problem Formulation

In Cartesian coordinates (x, y, z), let us consider the Poiseuille flow in an infinite duct of streamwise-uniform rectangular cross-section $\Sigma = \{(y,z) : -1 < y < 1, -A < z < A\}$, where $A \geq 1$ is the duct aspect ratio. The study of nonmodal temporal stability of this flow, which we will call basic, is reduced [7,8] to the analysis of solutions of the following form:

$$\mathbf{v}'(x,y,z,t) = \mathbf{v}(y,z,t)\mathrm{e}^{\mathrm{i}\alpha x}, \quad p'(x,y,z,t) = p(y,z,t)\mathrm{e}^{\mathrm{i}\alpha x}, \tag{1}$$

where i is the imaginary unit, $\alpha \geq 0$ is the streamwise wavenumber, t is the time and $\mathbf{v} = (u, v, w)^T$ and p are complex-valued amplitudes of the velocity and the pressure disturbances, respectively. These amplitudes satisfy the equations

$$\frac{\partial \mathbf{v}}{\partial t} = -(\mathbf{V}\cdot\nabla)\mathbf{v} - (\mathbf{v}\cdot\nabla_0)\mathbf{V} - \nabla p + \frac{1}{\mathrm{Re}}\nabla^2\mathbf{v}, \quad \nabla\cdot\mathbf{v} = 0 \tag{2}$$

in the domain Σ with no-slip (zero) boundary conditions for the velocity components. It is assumed that the initial condition for that system is a non-trivial, sufficiently smooth and divergence-free vector function, satisfying the no-slip boundary conditions. The system (2) is derived by substituting disturbances of the form (1) into the linearized (around the basic flow) equations of motion of a viscous incompressible fluid. Here, $\nabla = (\mathrm{i}\alpha, \partial/\partial y, \partial/\partial z)^T$, $\nabla_0 = (0, \partial/\partial y, \partial/\partial z)^T$, Re is the Reynolds number determined based on the duct half-height and the maximum velocity of the basic flow (the maximum being reached at the center of the cross-section), $\mathbf{V} = (U, 0, 0)^T$ is the velocity vector of the basic flow with normalized profile $U(y,z)$. It can be computed by solving the Poisson equation $\nabla_0^2 U = -1$ in the domain Σ with the no-slip conditions at the boundary and normalizing the solution to $U(0,0)$ [3,23].

Let us define the average kinetic energy density of the velocity disturbance (1) through its amplitude $\mathbf{v}$ as follows:

$$\mathcal{E}(\mathbf{v}') = \frac{\alpha}{16A\pi}\int\limits_{-\pi/\alpha}^{\pi/\alpha}\int\limits_{\Sigma}\mathbf{v}'\cdot\bar{\mathbf{v}}' dxdydz = \frac{1}{8A}\int\limits_{\Sigma}\mathbf{v}\cdot\bar{\mathbf{v}}dydz = \mathcal{E}(\mathbf{v}), \tag{3}$$

where the upper bar denotes the complex conjugation. When $\alpha = 0$, the disturbance amplitudes (1) are real, and when $\alpha > 0$ they are complex, but their real parts, $\mathrm{Real}\mathbf{v}' = (\mathbf{v}' + \bar{\mathbf{v}}')/2$, have physical meaning. It can be shown that $\mathcal{E}(\mathrm{Real}\mathbf{v}') = \mathcal{E}(\mathbf{v})/2$ when $\alpha > 0$.

Given (3), the maximum amplification of the average kinetic energy density of velocity disturbances of the form (1) for the linearized Equations (2) at fixed A, α and Re is the value

$$\Gamma_{\mathrm{Re}}^{A\alpha} = \sup\frac{\mathcal{E}(\mathbf{v}(t))}{\mathcal{E}(\mathbf{v}(0))},$$

where the supremum is taken over all $t \geq 0$ and all admissible initial disturbance amplitudes (i.e., nonzero, sufficiently smooth, divergence-free and satisfying the no-slip conditions on the duct wall). The initial disturbance displaying the maximum amplification $\Gamma_{\mathrm{Re}}^{A\alpha}$ is called optimal. We will assume $\mathcal{E}(\mathbf{v}(0)) = 1$, since for the linearized equations $\Gamma_{\mathrm{Re}}^{A\alpha}$ does not depend on the amplitude of initial disturbance [7].

For an arbitrary function $f(y,z)$ given in Σ, let us define functions of the form

$$f_{\diamond\circ}(y,z) = \frac{f(y,z)\circ f(y,-z)}{4}\diamond\frac{f(-y,z)\circ f(-y,-z)}{4},$$

where $\diamond$ and $\circ$ stand for $+$ or $-$. That is, for example, the function f_{-+} is odd in y and even in z. Given that $U(y,z)$ is even [3] in y and z, it can be shown that if (u,v,w,p) is a solution to the system (2) at given A, α and Re, then the following four sets of functions:

$$\begin{array}{ll} \mathbf{I}\ (u_{-+}, v_{++}, w_{--}, p_{-+}), & \mathbf{II}\ (u_{++}, v_{-+}, w_{+-}, p_{++}), \\ \mathbf{III}\ (u_{--}, v_{+-}, w_{-+}, p_{--}), & \mathbf{IV}\ (u_{+-}, v_{--}, w_{++}, p_{+-}), \end{array} \tag{4}$$

also satisfy this system. Thus, the solution of the system (2) can be reduced to a separate search for solutions possessing one of the four symmetries (4). It will be shown below that taking into account the symmetries (4) allows one to reduce the computation of the solution to the system (2) to computations in a quarter of the domain Σ. Note that in the square duct the solutions of symmetry I pass to those of symmetry IV if the duct is rotated through $\pi/2$ about its streamwise axis.

2.2. Computation Technique

Using the collocation method based on Legendre polynomials [25], we approximate the system (2) in space as in the work [3] with the Gauss–Lobatto nodes for the velocity and the Gauss nodes for the pressure. As a result, we obtain the system

$$\frac{d\mathbf{v}}{dt} = J\mathbf{v} + G\mathrm{p}, \quad F\mathbf{v} = 0 \tag{5}$$

with matrices $J \in \mathbb{C}^{n_\mathrm{v}\times n_\mathrm{v}}$, $G \in \mathbb{C}^{n_\mathrm{v}\times n_\mathrm{p}}$, $F \in \mathbb{C}^{n_\mathrm{p}\times n_\mathrm{v}}$, where $n_\mathrm{v} = 3n_y n_z$, $n_\mathrm{p} = (n_y+1)(n_z+1)$, and n_y and n_z are the numbers of internal nodes for approximating the velocity components in the directions y and z, respectively. In addition, $\mathbf{v}$ is the n_v-component column vector, which contains values of the velocity components in the internal Gauss–Lobatto nodes, and p is the n_p-component column vector, which contains values of the pressure in the Gauss nodes.

Using the Gauss–Lobatto quadratures [25], the discrete analog of the functional (3) can be written in the form: $\mathcal{E}(\mathbf{v}) = (E^2\mathbf{v},\mathbf{v})$, where $E = K_z \otimes K_y$, and K_z and K_y are diagonal matrices, containing the square roots of the Gauss–Lobatto weights in the y and z directions, respectively ($\otimes$ denotes the Kronecker product). Let us change the variables $\mathbf{v} := E\mathbf{v}/\sqrt{8A}$, $\mathrm{p} := E_\mathrm{p}\mathrm{p}/\sqrt{8A}$, $J := EJE^{-1}$, $G := EGE_\mathrm{p}^{-1}$, $F := E_\mathrm{p}FE^{-1}$, where $E_\mathrm{p} = K_{\mathrm{p}z} \otimes K_{\mathrm{p}y}$, and $K_{\mathrm{p}z}$ and $K_{\mathrm{p}y}$ are diagonal matrices containing the square roots of Gauss weights [25] in y and z, respectively. As a result, $\mathcal{E}(\mathbf{v}) = \|\mathbf{v}\|_2^2$ and the matrices J, G and F will [3] satisfy the conditions $J = J^* < 0$ and $F = G^*$. Therefore, the system (5) can be written as follows:

$$\frac{d\mathbf{v}}{dt} = J\mathbf{v} + G\mathrm{p}, \quad G^*\mathbf{v} = 0. \tag{6}$$

The system (6) preserves at the discrete level the well-known property [3] of the equations of motion of viscous incompressible fluid , namely, the possibility to exclude the pressure using the continuity equation. Therefore, following the works [23,24], we orthogonally project the system onto a subspace of divergence-free grid functions. To this end, we need a rectangular unitary matrix Q of size $n_\mathrm{v} \times (n_\mathrm{v} - n_\mathrm{p})$, whose columns form an orthonormal basis in the kernel of the matrix G^*. The arbitrary vector $\mathbf{v}$ satisfying the second equation in (6) can be uniquely represented as $\mathbf{v} = Q\mathbf{u}$, where $\mathbf{u} = Q^*\mathbf{v}$. Multiplying the first equation in (6) by Q^*, we obtain an equivalent to (6) system of ordinary differential equations

$$\frac{d\mathbf{u}}{dt} = H\mathbf{u}, \tag{7}$$

with matrix $H = Q^*JQ$ of order $n = n_\mathrm{v} - n_\mathrm{p}$, i.e., approximately half the algebraic dimension of the system (6). Note that the matrix Q can be computed based on the QR-decomposition [26] of the matrix G.

Let $\mathbf{v}(t,\mathbf{v}^0)$ be the solution to the Cauchy problem for the system (6) for fixed A, α and Re with an initial condition $\mathbf{v}^0$. We will assume asymptotic Lyapunov stability of this system, that is, $\|\mathbf{v}(t,\mathbf{v}^0)\|_2 \to 0$ at $t \to \infty$. A vector $\mathbf{v}^0$ is called the optimal disturbance if $\max\{\mathcal{E}(\mathbf{v}(t,\mathbf{v}^0)) : t \ge 0, G^*\mathbf{v}^0 = 0, \mathcal{E}(\mathbf{v}^0) = 1\}$ is the largest among all admissible $\mathbf{v}^0$. We will restrict ourselves to optimal disturbances on which this maximum is achieved at the smallest t, i.e., at

$$t_\mathrm{opt} = \min \arg \max_{t\ge 0} \Gamma_{\mathrm{Re}}^{A\alpha}(t),$$

where $\Gamma_{\mathrm{Re}}^{A\alpha}(t) = \max\{\mathcal{E}(\mathbf{v}(t;\mathbf{v}^0)) : G^*\mathbf{v}^0 = 0, \mathcal{E}(\mathbf{v}^0) = 1\}$ is the maximum amplification of the average kinetic energy density of disturbances at given t, A, α, Re and arg max stand for the argument of the maximum (i.e., the values of t at which $\Gamma_{\mathrm{Re}}^{A\alpha}(t)$ is maximized). One can show [23] that $\mathcal{E}(\mathbf{v}(t;\mathbf{v}^0)) = \|\exp\{tH\}\mathbf{u}^0\|_2^2$, where $\mathbf{u}^0 = Q^*\mathbf{v}^0$. Thus,

$$\Gamma_{\mathrm{Re}}^{A\alpha}(t) = \|\exp\{tH\}\|_2^2, \quad \Gamma_{\mathrm{Re}}^{A\alpha} = \Gamma_{\mathrm{Re}}^{A\alpha}(t_\mathrm{opt}).$$

Hence, the computation of $t_{\rm opt}$ and the optimal disturbance is reduced to computing the norm of the matrix exponential at various t. To this end, we will use the original algorithm [27]. Then, $\mathbf{v}^0_{\rm opt} = \sqrt{8A}E^{-1}Q\mathbf{u}^0_{\rm opt}$ is the sought optimal disturbance, where

$$\mathbf{u}^0_{\rm opt} \in \arg\max_{\mathbf{u}^0\in\mathbb{C}^n} \|\exp\{t_{\rm opt}H\}\mathbf{u}^0\|_2, \quad \|\mathbf{u}^0\|_2 = 1$$

is the right normalized singular vector [26] of the matrix $\exp\{t_{\rm opt}H\}$ corresponding to the maximum singular value. To compute this vector, the SVD-decomposition [26] of matrix $\exp\{t_{\rm opt}H\}$ is used.

It can be shown that the chosen approximation method and the subsequent transformations preserve the symmetries (4) of the solutions to the system (2). Let us describe their accounting for the symmetries. For simplicity, we assume that n_y and n_z are even. Let the vectors $\hat{\mathbf{v}} \in \mathbb{C}^{\hat{n}_{\rm v}}$ and $\hat{\rm p} \in \mathbb{C}^{\hat{n}_{\rm p}}$ contain values of $\mathbf{v}$ and p at nodes with $y \le 0$ and $z \le 0$, so $\hat{n}_{\rm v} = n_{\rm v}/4$, and $\hat{n}_{\rm p} = n_y/2(n_z/2+1)$, $(n_y/2+1)(n_z/2+1)$, $n_yn_z/4$ and $(n_y/2+1)n_z/2$ for symmetries I–IV, respectively. For each symmetry, we define a rectangular block-diagonal matrix S with the blocks being matrices of the form $S_{\diamond\circ} = S^z_\circ \otimes S^y_\diamond$ and the rectangular matrix $S_{\rm p} = S^z_{{\rm p}\circ} \otimes S^y_{{\rm p}\diamond}$, where $\diamond$ and $\circ$ stand for $+$ or $-$ and are chosen according to (4). For example, $S = \mathrm{diag}(S_{-+}, S_{++}, S_{--})$ and $S_{\rm p} = S^z_{{\rm p}+} \otimes S^y_{{\rm p}-}$ for symmetry I; furthermore, e.g.,

$$S^y_\diamond = \begin{bmatrix} I_{n_y/2} \\ \diamond I'_{n_y/2} \end{bmatrix}, \quad S^y_{{\rm p}+} = \begin{bmatrix} I_{n_y/2} & 0 \\ 0 & 1 \\ I'_{n_y/2} & 0 \end{bmatrix}, \quad S^y_{{\rm p}-} = \begin{bmatrix} I_{n_y/2} \\ 0 \\ -I'_{n_y/2} \end{bmatrix},$$

where I_n and I'_n are the identity matrix and anti-diagonal identity matrix of order n, respectively, and 0 is a zero matrix of appropriate dimension. Hence, $\mathbf{v} = S\hat{\mathbf{v}}$ and ${\rm p} = S_{\rm p}\hat{\rm p}$. Then, by scaling the symmetry matrices $S := S/2$ (after which the matrix S is orthogonal), $S_{\rm p} := S_{\rm p}/2$, we perform the change of variables $J := S^TJS$, $G := S^TGS_{\rm p}$, $\hat{\mathbf{p}} := 2\hat{\mathbf{p}}$. As a result, we obtain four independent systems of the form (6) with respect to $\hat{\mathbf{v}}$ and $\hat{\rm p}$, whose solutions will be pairwise orthogonal. Further, these systems can be reduced to that of the form (7). Considering that the algorithm [27] used to compute the norm of the matrix exponential requires about $\mathcal{O}(n^3)$ floating-point operations, then taking symmetries into account allows one to reduce the number of operations by a factor of about 64. It should be also noted that one of the advantages of the described numerical model is the use of standard matrix algorithms (like QR or SVD decompositions) implemented in LAPACK library and bundled, e.g., with MATLAB.

3. Results

The following ranges of values of the configuration parameters were considered: the aspect ratio, $1 \le A \le 8$, the streamwise wavenumber, $0 \le \alpha \le 1.0$, the Reynolds number, $1000 \le \mathrm{Re} \le 4000 < \mathrm{Re_L}(A)$, where the dependence $\mathrm{Re_L}(A)$ of the linear critical Reynolds number on A can be found in [2,3]. The computations were performed taking into account the disturbance symmetries on grids with $n_y = 20$ and 40, and $n_z = \lfloor An_y \rfloor$, where $\lfloor a \rfloor$ denotes the integer part of the number a. The grid $20 \times \lfloor 20A \rfloor$ provided grid convergence of the results with sufficient accuracy, so the results obtained on this grid are presented below.

For given A and Re, we define the maximum amplification of the average kinetic energy density of disturbances as follows:

$$\Gamma^A_{\rm Re} = \max_{0\le\alpha\le1} \Gamma^{A\alpha}_{\rm Re}.$$

Figure 1 shows the isoines of $\Gamma^A_{\rm Re}$. Analysis of these data shows that $\Gamma^A_{\rm Re}$ grows monotonically at a fixed A with increasing Re and non-monotonically at a fixed Re with increasing A. The optimal disturbances displaying $\Gamma^A_{\rm Re}$ possess symmetry II at $A = 1$ (while the disturbances of symmetries I and IV show almost the same maximum amplification) and symmetries I or III alternately at $A > 1$.

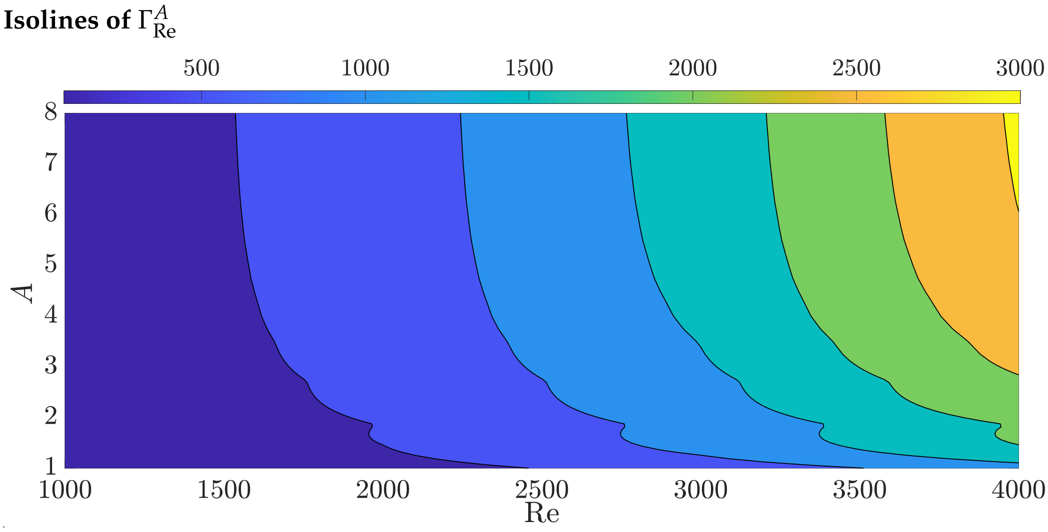

Figure 1. Isolines of Γ_{Re}^{A} equally spaced by 500. The optimal disturbances possess $\alpha = 0$, symmetry II for $A = 1$ and I or III alternately for $A > 1$.

Figure 2 shows a typical view of the dependence Γ_{Re}^{A} at a fixed Re for disturbances of each symmetry. It can be seen that the non-monotonicity of the maximum possible amplification is related, on the one hand, to the change of the symmetry of the optimal disturbance from I to III and vice versa (in particular, at $A \approx 1.9$, 2.8, and 3.5). On the other hand, the dependences Γ_{Re}^{A} for symmetries I, II, and IV are non-monotonic themselves, at least at relatively small A. To explain this, the corresponding optimal disturbances of each symmetry were studied. The computations have shown that such disturbances are streamwise uniform counter-rotating vortices; i.e., they have $\alpha = 0$. Below, we discuss the projections of real parts of the initial amplitudes $\mathbf{v}_{\mathrm{opt}}^{0}$ of the optimal disturbances (hereafter, for brevity, optimal disturbances) onto the duct cross-section.

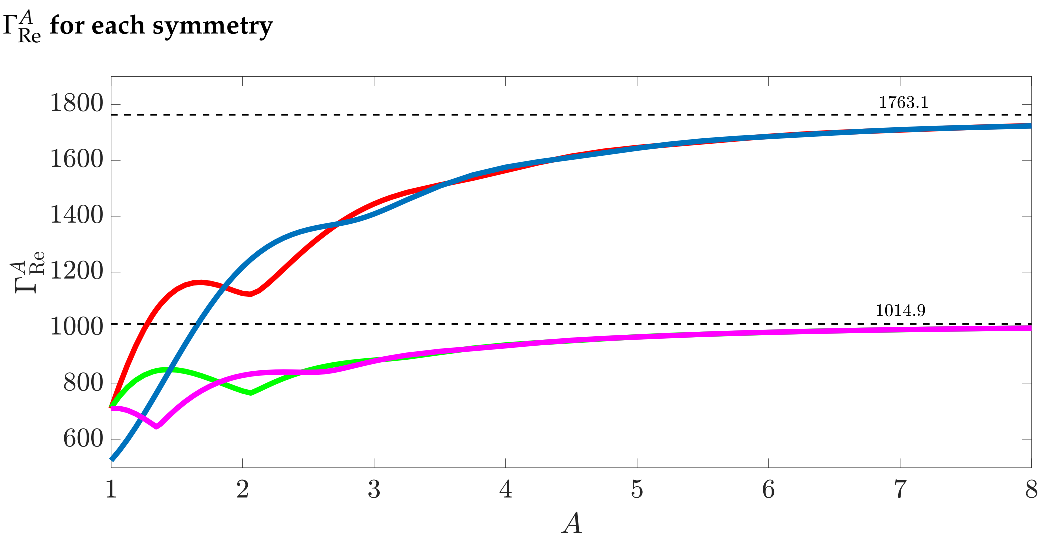

Figure 2. Dependences Γ_{Re}^{A} for each symmetry (I is red, II is green, III is blue, IV is purple); Re = 3000. The optimal disturbances possess $\alpha = 0$ for all symmetries. Dashed lines correspond to the maximum amplification for the plane Poiseuille flow at Re = 3000 for symmetries (8): the upper line corresponds to symmetry I; the lower line corresponds to symmetry II.

Figure 3 shows a typical view of the optimal disturbances of all four symmetries. Let us discuss their features at $A = 1$. The optimal disturbances of symmetries I and IV consist of two vortices. Such disturbances coincide if the duct is rotated through $\pi/2$ about its streamwise axis, so they display the same amplifications Γ^A_{Re}. The optimal disturbances of symmetries II and III consist of four vortices: in the former the vortices are located in each quarter of the cross-section, and in the latter they are located at the cross-section axes. The optimal disturbances of symmetry II show a noticeably larger amplification Γ^A_{Re}. Apparently, this is because a sufficiently intense vortex motion, which mixes different layers of the fluid and, thereby, causes a growth of the disturbance streamwise velocity (the so-called lift-up effect [28,29]), occurs almost in the entire cross-section for the optimal disturbances of symmetry II, while for that of symmetry III such motion occurs only near the cross-section axes.

Optimal disturbances for each symmetry

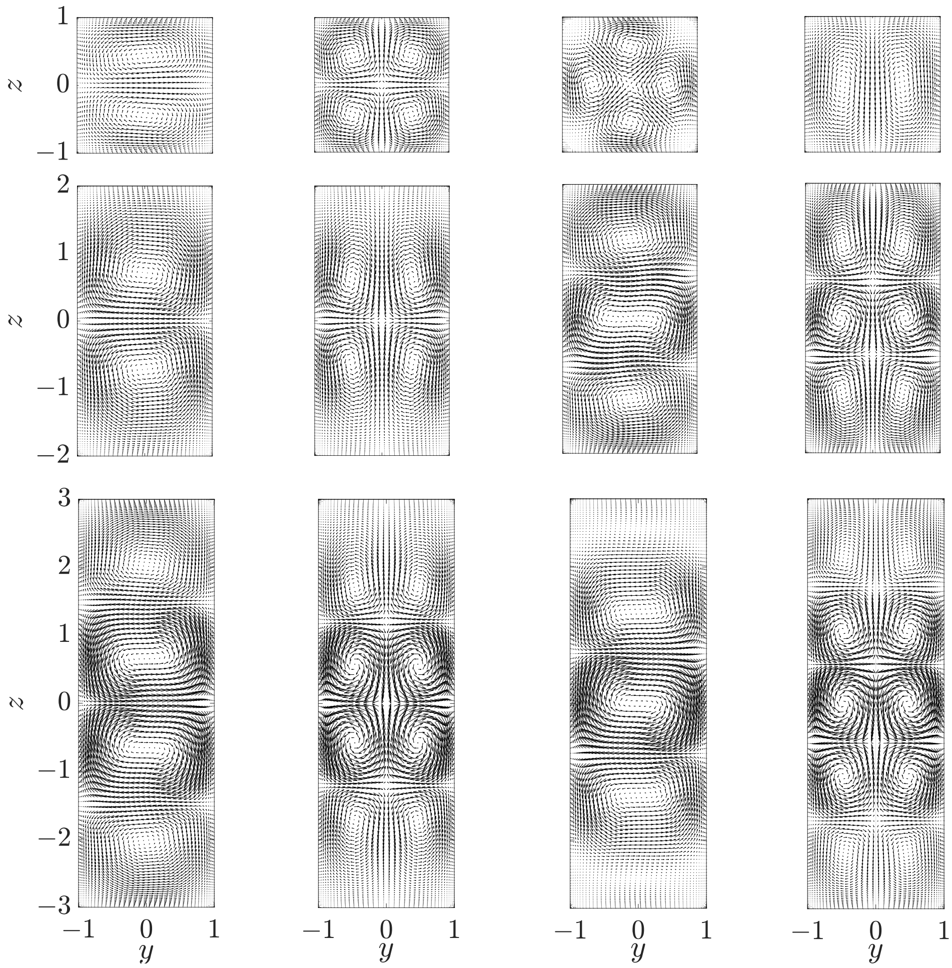

Figure 3. Optimal disturbances at $t = 0$ for $A = 1$, 2 and 3 (rows 1–3), possessing symmetries I–IV (columns from left to right).

The growth of A is accompanied, first, by a change in the shape of the vortices comprising the optimal disturbances. In particular, the vortex width grows, which we denote by $\tilde{A}$. Second, by a change in the number of vortices. For symmetries I, II and IV, this number grows, remaining even. For symmetry III, the optimal disturbance consists of four vortices at $A = 1$, but as A grows, the upper and lower vortices merge initially (thereby the number became odd), and then the number of vortices increases, remaining odd. The optimal disturbances of symmetries I and III (at $A \gtrsim 2$) consist of one row of vortices, and those of symmetries II and IV consist of two rows. This, apparently, explains the tendency of Γ^{A}_{Re} values for symmetries I and III and symmetries II and IV, respectively, to converge to each other with increasing A (see Figure 2).

It turns out that an increase in the number of vortices of the optimal disturbance means that instead of a disturbance that was optimal at some A, another disturbance consisting of a larger number of vortices becomes optimal with increasing A. Let us illustrate this for disturbances of symmetry I. At $A = 2$, in addition to the optimal disturbance (*1* in Figure 4) consisting of two vortices, there are disturbances that exhibit lower energy amplification and consist of more vortices. For example, disturbance *2* in Figure 4 contains four vortices, although two of them are relatively weakly developed, and is optimal at $t \approx 187 < t_{\mathrm{opt}} \approx 240$. However, when $A = 2.2$, such disturbance becomes optimal.

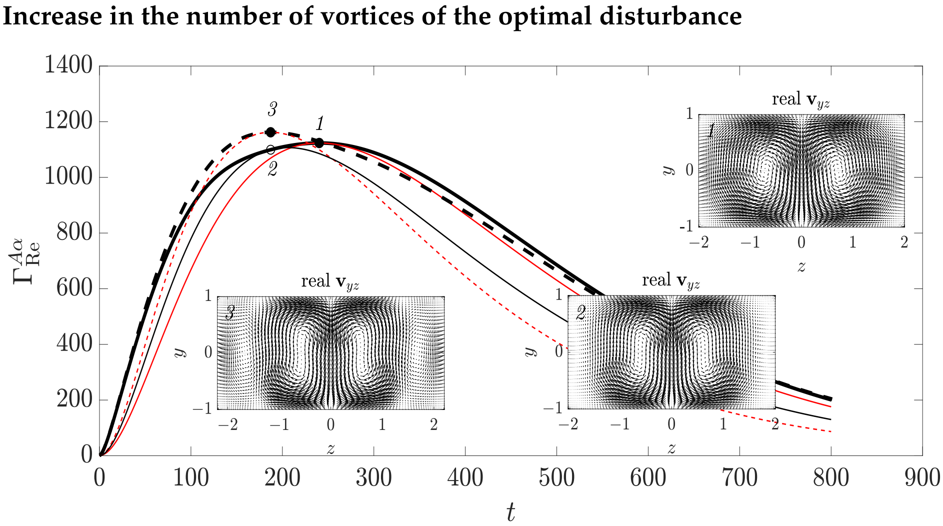

Figure 4. Dependence $\Gamma^{A\alpha}_{\mathrm{Re}}(t)$ for $A = 2$ (black line) and 2.2 (dashed black line) and also the amplification of kinetic energy of the corresponding optimal disturbances (*1* and *3*, red) and of the disturbance *2*, gray), which is optimal at $A = 2$ and $t \approx 187$; $\alpha = 0$, Re $= 3000$, symmetry I.

It follows from the obtained results that the change in the symmetry of the optimal disturbance observed with increasing A is a consequence of an increase in the number of vortices that comprise the disturbance (an even number is substituted by an odd number and, accordingly, symmetry I is substituted by symmetry III). In addition, the computations have shown that the increase in the number of vortices of the optimal disturbance first occurs at $A \approx 2.1$ and further at $A \approx 3.7$ for symmetry I, at $A \approx 2.1$ and 3.2 for symmetry II, at $A \approx 2.9$ and 4.4 for symmetry III, at $A \approx 1.4$ and 2.6 for symmetry IV. That is, the changes in the behavior of Γ^{A}_{Re} for a given symmetry (see Figure 2: for symmetries I, II and IV, the decrease of Γ^{A}_{Re} is substituted by an increase, and for symmetry III, the growth rate of Γ^{A}_{Re} increases) are also associated with the increase in the number of vortices.

Therefore, to explain the dependence Γ^{A}_{Re}, it remains to understand how A affects the amplification of the optimal disturbance with $\alpha = 0$ consisting of a fixed number of vortices. To this end, we additionally consider optimal disturbances of the plane Poiseuille flow with $\alpha = 0$ and $\beta > 0$, where β is the transverse wavenumber. Such disturbances also consist of streamwise counter-rotating vortices (see [7,8,30]). It is natural to assume that the effect of A on the amplification of the above-mentioned optimal disturbance in a rectangular duct should be qualitatively the same as the effect of the transverse wavelength $2\pi/\beta$ of the optimal disturbance on its amplification in a plane channel, since both of these parameters determine the width of the disturbance vortices.

Figure 5 shows the isolines of the maximum amplification $\Gamma^{\beta}_{\mathrm{Re}}$ of the average kinetic energy density of disturbances of the plane Poiseuille flow. The computations were performed for $0 \leq \alpha \leq 1$, $0 \leq \beta \leq 4$ and $1000 \leq \mathrm{Re} \leq 4000$ based on the present model, taking into account two possible symmetries of disturbances with respect to the horizontal axis:

$$\mathbf{I}\ (u_-, v_+, w_-, p_-), \qquad \mathbf{II}\ (u_+, v_-, w_+, p_+). \tag{8}$$

It turns out that for each symmetry $\Gamma^{\beta}_{\mathrm{Re}}$ has a maximum that is achieved on the optimal disturbances (see Figure 6) with $\alpha = 0$ and some Re-independent wavenumber $\beta = \beta_\infty > 0$, where $\beta_\infty \approx 2.0$ for symmetry I and 2.6 for symmetry II. In other words, for a given symmetry, the maximum amplification is displayed by the optimal disturbances with the transverse wavelength of $2\pi/\beta_\infty$, i.e., consisting of vortices of width

$$\tilde{A}_\infty = \pi/\beta_\infty, \tag{9}$$

since the wavelength of these disturbances contains two vortices or two pairs of vortices.

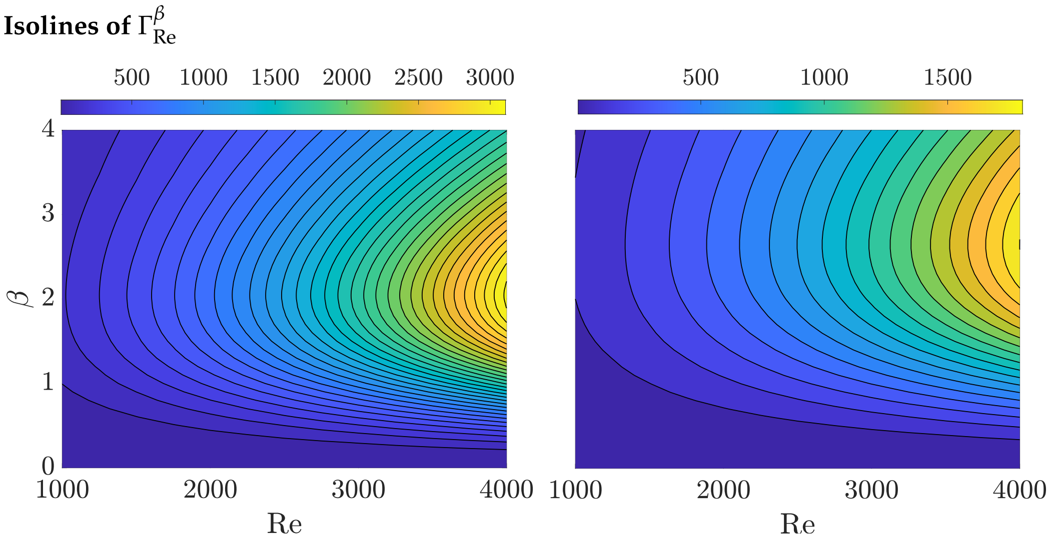

Figure 5. Isolines of $\Gamma^{\beta}_{\mathrm{Re}}$ for the plane Poiseuille flow equally spaced by 100 for symmetry I (**left**) and II (**right**). The optimal disturbances possess $\alpha = 0$. The maximum of $\Gamma^{\beta}_{\mathrm{Re}}$ is achieved at $\beta = \beta_\infty$, where $\beta_\infty = 2.044$ for symmetry I and 2.6 for symmetry II.

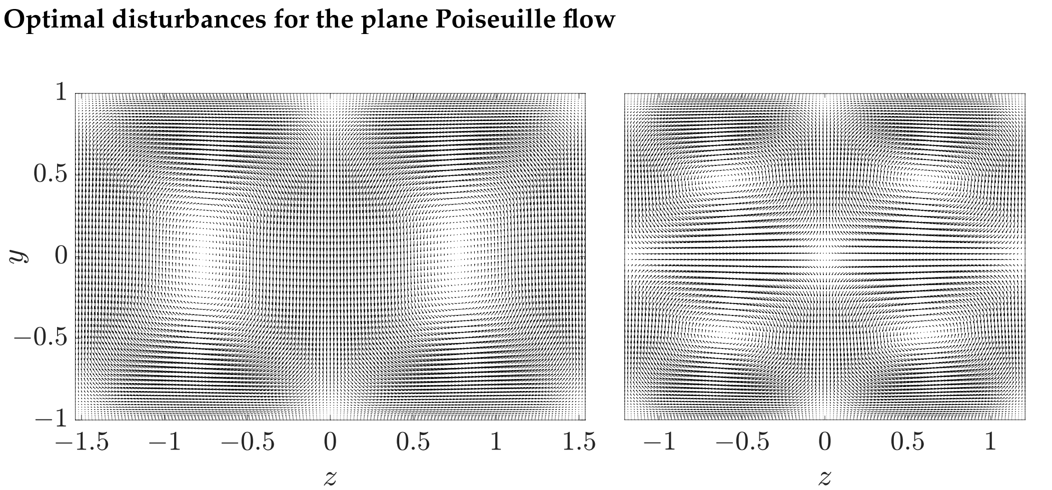

Figure 6. Optimal disturbances of symmetry I (**left**) and II (**right**) for the plane Poiseuille flow (one period of disturbances is shown), displaying the maximum of $\Gamma^{\beta}_{\mathrm{Re}}$ shown in Figure 5.

Thus, in a rectangular duct, the optimal disturbance with $\alpha = 0$ consisting of a certain number of vortices will display the largest amplification at a certain aspect ratio A_*, which depends on the number of vortices. Any deviation (oversizing or undersizing) of A from A_* will decrease the amplification of such disturbance just as $\Gamma_{\mathrm{Re}}^{\beta}$ decreases in the plane channel when the transverse wavelength of the disturbance deviates from the value $2\pi/\beta_\infty$. Thus, for a given symmetry, the non-monotonicity of Γ_{Re}^{A} arises, apparently, only when the further increase in the number of vortices of the optimal disturbance occurs at $A > A_*$.

For sufficiently small values of A, the optimal disturbance of any symmetry, excluding III (for which at $1 \leq A \lesssim 2$ the vortices merge), consists of the minimum possible number of vortices, which, like in the optimal disturbances in the plane channel, have the same width. Therefore, it can be assumed that for such a disturbance

$$A_* \approx N\tilde{A}_\infty/2, \tag{10}$$

where N is the number of vortices of the disturbance of symmetry I or the number of vertical pairs of vortices of the disturbance of symmetry II or IV, and $\tilde{A}_\infty$ is calculated by the formula (9) using the corresponding value of β_∞. Given that the vortices of the optimal disturbance of symmetry I in the rectangular duct tend in shape and size with increasing A to the vortices of the optimal disturbance of symmetry I in the plane channel, then $\tilde{A}_\infty \approx 1.5$ for them in (10). The same is true for the disturbances of symmetries II and IV in the rectangular duct and symmetry II in the plane channel, i.e., $\tilde{A}_\infty \approx 1.2$ for them.

Let us examine how the values of A_* estimated by (10) agree with the locations of the local maxima of the dependence Γ_{Re}^{A} (Figure 2) for disturbances of symmetries I, II and IV (Figure 3). The optimal disturbance of symmetry I consists at $1 \leq A \lesssim 2.1$ of two vortices, i.e., $N = 2$, so $A_* \approx 1.5$. This value agrees reasonably well with the computed value of $A \approx 1.7$, at which a local maximum of Γ_{Re}^{A} is observed. The optimal disturbance of symmetry II consists at $1 \leq A \lesssim 2.1$ of two pairs of vortices, i.e., $N = 2$, so $A_* \approx 1.2$. This value also agrees reasonably well with the computed value $A \approx 1.4$. Finally, the optimal disturbance of symmetry IV consists at $1 \leq A \lesssim 1.4$ of one pair of vortices, that is, $N = 1$, so $A_* \approx 0.6$. Consequently, increasing A in the range $1 \leq A \lesssim 1.4$ should lead to the decrease of the amplification up to $A \approx 1.4$, at which the number of vortices of the optimal disturbance increases, which is in good agreement with the obtained results.

For sufficiently large A, the estimate (10) will be rougher. This is due to the fact that it is based on the assumption that all vortices of the optimal disturbance have the same width $\tilde{A}_\infty$. However, after the number of vortices of the optimal disturbance has been increased, their widths turn out to be unequal. This is clearly visible for disturbances of all symmetries, e.g., when $A = 3$. Nevertheless, this estimate still predicts an increase in Γ_{Re}^{A} for disturbances of symmetries I, II and IV, which is observed (Figure 2) starting from values $A \approx 2.1$, 2.1 and 1.4, respectively, at which the increase in the number of their vortices occurred, since A_* for these disturbances exceeds the indicated values of A and is approximately equal to 3.1, 2.4 and 1.8, respectively.

4. Conclusions

The Poiseuille flow in an infinite duct of streamwise-uniform rectangular cross-section is considered in this paper. The results of numerical parametric analysis of the temporal nonmodal stability of this flow are presented. In particular, the dependence of the maximum amplification Γ_{Re}^{A} of the average kinetic energy density of disturbances on the aspect ratio $1 \leq A \leq 8$ and the Reynolds number $1000 \leq \mathrm{Re} \leq 4000$, as well as the optimal disturbances by which Γ_{Re}^{A} is achieved, are computed. All computations have been performed taking into account four possible symmetries with respect to the cross-section axes that are allowed by the solutions of the linearized equations for the disturbance amplitudes. The following conclusions can be drawn on the basis of the obtained results.

The value of Γ_{Re}^{A} grows significantly both with increasing Re and with increasing A and in the latter case non-monotonically. Namely, Γ_{Re}^{A} increases with A in the entire considered range of A except $1.7 \lesssim A \lesssim 1.9$. That is, the increase in the aspect ratio promotes the subcritical laminar–turbulent transition in almost the entire considered range of A. Therefore, an increase in the aspect ratio is necessary if an enhancement of the flow vorticity is preferable and vice versa.

The optimal disturbances by which Γ^A_{Re} is achieved are streamwiseuniform counter-rotating vortices. An increase in A is accompanied, first, by a change in the shape of the vortices. In particular, their width grows. Second, by an increase in the number of vortices. The latter means that instead of the disturbance, which was optimal at some A, another disturbance consisting of a larger number of vortices becomes optimal with increasing A. Along with the increase of the number of vortices, the symmetry of the optimal disturbance changes.

As a result, the explanation of the dependence of Γ^A_{Re} on A is reduced to that of the influence of A on the amplification of the optimal disturbance consisting of some fixed number of vortices. It is assumed in the paper that this influence of A should be qualitatively the same as the influence of the transverse wavelength of the optimal disturbance on its amplification in the plane channel flow, since both these parameters determine the width of the disturbance vortices. Based on this assumption, a qualitative explanation of the dependence of Γ^A_{Re} on A is proposed.

Concluding, it is worth noting that further research that can be carried out on this subject is manifold. In particular, an extension to consider effects of heating/cooling of the duct walls (typical, e.g., for heat exchangers) that often ccurs in practice, or nanoparticle additives on the nonmodal stability of the basic flow, is reasonable.

Author Contributions: Conceptualization, A.B. and K.D.; methodology, A.B. and K.D.; investigation, K.D. and N.K.; writing (original draft preparation), K.D.; writing (review and editing), A.B. and K.D.; visualization, N.K.; software, K.D.; validation, N.K. All authors have read and agreed to the published version of the manuscript.

Funding: This research was funded by Russian Science Foundation grant number 22-71-10028.

Institutional Review Board Statement: Not applicable.

Data Availability Statement: The data that support the findings of this study are available within the article.

Acknowledgments: The authors are grateful to the anonymous reviewers for their careful reading of the manuscript and valuable comments, which allowed the authors to improve the work.

Conflicts of Interest: The authors declare no conflict of interest. The funders had no role in the design of the study; in the collection, analyses, or interpretation of data; in the writing of the manuscript; or in the decision to publish the results.

References

1. Drazin, P.G.; Reid, W.H. *Hydrodynamic Stability*, 2nd ed.; Cambridge University Press: Cambridge, UK, 2004.
2. Tatsumi, T.; Yoshimura, T. Stability of the laminar flow in a rectangular duct. *J. Fluid Mech.* **1990**, *212*, 437–449. [CrossRef]
3. Demyanko, K.V.; Nechepurenko, Y.M. Linear stability analysis of Poiseuille flow in a rectangular duct. *Russ. J. Numer. Anal. Math. Model.* **2013**, *28*, 125–148. [CrossRef]
4. Orszag, S.A. Accurate solution of the Orr–Sommerfeld stability equation. *J. Fluid Mech.* **1971**, *50*, 689–703. [CrossRef]
5. Kerswell, R.R.; Davey, A. On the linear instability of elliptic pipe flow. *J. Fluid Mech.* **1996**, *316*, 307–324. [CrossRef]
6. Demyanko, K.; Klyushnev, N. On monotonic stability of elliptic pipe flow. *Phys. Fluids* **2021**, *33*, 114108. [CrossRef]
7. Schmid, P.J.; Henningson, D.S. *Stability and Transition in Shear Flows*; Springer New York: New York, NY, USA, 2000.
8. Boiko, A.V.; Dovgal, A.V.; Grek, G.R.; Kozlov, V.V. *Physics of Transitional Shear Flows*; Springer: Dordrecht, The Netherlands, 2012.
9. Reddy, S.C.; Schmid, P.J.; Henningson, D.S. Pseudospectra of Orr–Sommerfeld operator. *SIAM J. Appl. Math.* **1993**, *53*, 15–47. [CrossRef]
10. Reddy, S.C.; Henningson, D.S. Energy growth in viscous channel flows. *J. Fluid Mech.* **1993**, *252*, 209–238. [CrossRef]
11. Trefethen, L.N.; Trefethen, A.E.; Reddy, S.C.; Driscoll, T.A. Hydrodynamic stability without eigenvalues. *Science* **1993**, *261*, 578–584. [CrossRef]
12. Schmid, P.J.; Henningson, D.S. Optimal energy density growth in Hagen–Poiseuille flow. *J. Fluid Mech.* **1994**, *277*, 197–225. [CrossRef]
13. Bottaro, A.; Corbett, P.; Luchini, P. The effect of base flow variation on flow stability. *J. Fluid Mech.* **2003**, *476*, 293–302. [CrossRef]
14. Schmid, P. Nonmodal stability theory. *Annu. Rev. Fluid Mech.* **2007**, *39*, 129–162. [CrossRef]

15. Kerswell, R. Nonlinear nonmodal stability theory. *Annu. Rev. Fluid Mech.* **2018**, *50*, 319–345. [CrossRef]
16. Rohsenow, W.M.; Hartnett, J.P.; Cho, Y.I. *Handbook of Heat Transfer*, 3rd ed.; McGraw-Hill: New York, NY, USA, 1998.
17. Garimella, S.; Dowling, W.; van der Veen, M.; Killion, J. The effect of simultaneously developing flow on heat transfer in rectangular tubes. *Heat Transf. Eng* **2001**, *22*, 12–25. [CrossRef]
18. Bennett, T. Laminar convection in rectangular ducts of fully developed flow. *Int. J. Heat Mass Transf.* **2020**, *156*, 119846. [CrossRef]
19. Dmitrienko, A. Stochastic equations for continuum and determination of hydraulic drag coefficients for smooth flat plate and smooth round tube with taking into account intensity and scale of turbulent flow. *Contin. Mech. Thermodyn.* **2017**, *29*, 1–9. [CrossRef]
20. Dmitrienko, A. Theoretical calculation of the laminar–turbulent transition in the round tube on the basis of stochastic theory of turbulence and equivalence of measures. *Contin. Mech. Thermodyn.* **2022**, *34*, 1375–1392. [CrossRef]
21. Criminale, W.; Jackson, T.; Lasseigne, D.; Joslin, R. Perturbation dynamics in viscous channel flows. *J. Fluid Mech.* **1997**, *339*, 55–75. [CrossRef]
22. Lasseigne, D.; Joslin, R.; Jackson, T.; Criminale, W. The transient period for boundary layer disturbances. *J. Fluid Mech.* **1999**, *381*, 89–119. [CrossRef]
23. Boiko, A.V.; Nechepurenko, Y.M. Numerical spectral analysis of temporal stability of laminar duct flows with constant cross-sections. *Comput. Math. Math. Phys.* **2008**, *48*, 1699–1714. [CrossRef]
24. Nechepurenko, Y.M. On the dimension reduction of linear differential-algebraic control systems. *Dokl. Math.* **2012**, *86*, 457–459. [CrossRef]
25. Canuto, C.; Hussaini, M.Y.; Quarteroni, A.; Zang, T.A. *Spectral Methods: Fundamentals in Single Domains*; Springer: Berlin, Germany, 2006.
26. Golub, G.; van Loan, C. *Matrix Computations*, 3rd ed.; The John Hopkins University Press: London, UK, 1996.
27. Nechepurenko, Y.M.; Sadkane, M. A low-rank approximation for computing the matrix exponential norm. *SIAM J. Matrix Anal. Appl.* **2011**, *32*, 349–363. [CrossRef]
28. Landahl, M.L. Wave breakdown and turbulence. *SIAM J. Appl. Math.* **1975**, *28*, 735–756. [CrossRef]
29. Landahl, M.L. A note on an algebraic instability of inviscid parallel shear flows. *J. Fluid Mech.* **1980**, *98*, 243–251. [CrossRef]
30. Butler, K.M.; Farrell, B.F. Three-dimensional perturbations in viscous shear flow. *Phys. Fluids A* **1992**, *4*, 1627–1650. [CrossRef]